Phase transition and high-pressure behavior of divalent metal oxides

K. N. Jog,* R. K. Singh,† and S. P. Sanyal
Condensed Matter Research Centre, Department of Post Graduate Studies and Research in Physics, Rani Durgawati University, Jabalpur 482001, Madhya Pradesh, India
(Received 8 August 1984)

The phase transition, relative stability, and high-pressure elastic behavior of alkaline-earth and transition-metal oxides have been successfully predicted by means of two well-known model potentials developed by Sangster and Stoneham and by Mackrodt and Stewart. The phase-transition pressures for these oxides are predicted to lie in the range 85 to 202 GPa. The relative volume changes corresponding to these transition pressures occur from 3.3% to 6.5%. Our results for transition pressures are higher than the available experimental data. However, the transition pressure from $B1$ to $B2$ structures increases with decreasing cation—to—anion-radii ratio at least qualitatively as the trend shown by the current data available for some of these oxides. The variation of elastic constants with pressure predicted from these models followed the same trend as that revealed by modified-electron-gas-model theory. The ratio of shear-to-bulk modulus at the predicted transition pressure for these oxides lies between 0.06 to 0.22. The discrepancies between theoretical and experimental results have been ascribed to the many-body interactions which are significantly important in ionic crystals.

I. INTRODUCTION

In recent years the study of phase-transition and high-pressure behavior of divalent metal oxides has attracted the attention of many workers,[1–11] as they are very useful and interesting materials from geophysical, academic, and technological points of view. Many of the oxide phases of the earth's mantle are known to undergo transformations at pressures occurring within the first few kilometers of depth, and the effect of such transformations upon seismologically observed properties is still not fully understood.[3] These oxides are also very interesting from a theoretical point of view, as they provide a link between the highly ionic alkali halides and the largely covalent III-V compound semiconductors. Besides these interests, oxides are of significant technological importance, since they become useful in laser developments when doped with transition elements.[12]

A considerable interest has been shown in developing accurate theoretical models to describe the high-pressure behavior of ionic crystals and in particular, oxides. This is largely due to the fact that the transition pressures for oxides are very high and they are accessible experimentally only by the shock-wave methods.[1] As indicated by Cohen and Gordon[1] these methods are not always reliable since their data correspond neither to an adiabatic nor to an isothermal compression. Earlier a modified electron-gas (MEG) model[1] had been applied to predict the nature of high- and low-pressure phases of some oxides.[1,13] The transition pressure for SrO (Ref. 13) obtained from the MEG model differs from its observed value[3] by about 100 GPa. However, there is small discrepancy between MEG calculations and the observed transition pressure for CaO.[6] Furthermore, the volume decrease at the $B1$-to-$B2$ transition for SrO is in excellent agreement with Jeanloz's results[3] from a model based on interatomic potentials. The situation stated above indicates that both *a priori* MEG (Ref. 1) and interionic potential[3] models cannot describe satisfactorily the high-pressure behavior of these oxides. Also, due to some practical limitations of attaining extraordinarily high pressure, the behavior of these oxides in the range 50 to 250 GPa could not be investigated properly. Thus there is still a need for accurate theoretical models to provide insight into the high-pressure (more than 50 GPa) behavior of these solids.

Motivated by this necessity, we thought it pertinent to study the pressure-induced phase-transition and high-pressure behavior of divalent (alkaline earth and transition) metal oxides, employing two well-known model potentials formulated by Sangster and Stoneham[14] and by Mackrodt and Stewart.[15] Earlier these models I and II (Refs. 14 and 15) have been used for the study of dynamic and defect properties of these oxides. The chief aim for the choice of these potentials is a critical assessment of the performance of these two potentials (Refs. 14 and 15) in predicting their phase-transition and high-pressure behavior. The parameters of model I (Ref. 14) have been obtained by fitting them to various experimental data, while the same parameters for model II (Ref. 15) have been determined from the *a priori* approach. In the present paper we have used these models to study the relative stability, phase-transition pressure, and volume and high-pressure elastic behavior of divalent metal oxides. A detailed description of these potentials is given elsewhere.[14,15] A brief account of their framework and the procedure adopted for calculation of the phase-transition pressure and the relative volume changes for $B1$-to-$B2$ transition are described in Secs. II and III. The high-

pressure elastic behavior has been presented in Sec. IV. The results computed from models I and II have been presented in Sec. V and discussed in Sec. VI.

II. INTERIONIC POTENTIALS

The important ionic solids crystallize in either rocksalt ($B1$) or cesium chloride ($B2$) structures. An isolated phase is stable only when its free energy is minimum for the specified thermodynamic conditions. As the temperature or pressure or any other variable acting on the systems is altered, the free energy changes smoothly and continuously. A phase transition is said to occur when the changes in structural details of the phase are caused by such variations of free energy. The divalent metal oxides transform from their initial $B1$ to $B2$ structure under pressure. The stability of a particular structure is decided by the minima of Gibbs free energy,

$$G = U + PV - TS \ , \tag{1}$$

where U is the internal energy, which at 0 K corresponds to the cohesive energy, S is the vibrational entropy at absolute temperature T, pressure P, and volume V.

The Gibbs free energies

$$G_{B1}(R) = U_{B1}(R) + 2PR^3 \tag{2}$$

for NaCl ($B1$) phase and

$$G_{B2}(R') = U_{B2}(R') + (8/3\sqrt{3})P(R')^3 \tag{3}$$

for CsCl ($B2$) phase become equal at the phase-transition pressure P and temperature 0 K. Here the abbreviations

$$U_{B1}(R) = -1.7476e^2Z^2/R + 6V_{+-}(R) + 6V_{++}(R) + 6V_{--}(R) \tag{4}$$

and

$$U_{B2}(R') = -1.7627e^2Z^2/R' + 8V_{+-}(R') + 3V_{++}(R') + 3V_{--}(R') \tag{5}$$

represent cohesive energies for $B1$ and $B2$ phases, respectively. Also, R and R' are the nearest-neighbor separations corresponding to these phases.

The short-range (SR) potentials (for $B1$ and $B2$ phases) between the ions are written as[14,15]

$$V_{ij}(r) = B_{ij}\exp(-r_{ij}/\rho_{ij}) - C_{ij}/r_{ij}^6, \quad i,j = +,- \tag{6}$$

where B_{ij} and ρ_{ij} are SR parameters and C_{ij} are van der Waals interaction coefficients. The SR parameters involved in model I (Ref. 14) have been determined by fitting them to the elastic, dielectric constants, and lattice spacing, and those of model II (Ref. 15) are obtained from the Clementi wave functions and Hartree-Fock calculations. The model I is an oversimplified model in which oxygen polarizability and interactions are taken to be the same for all oxides and cation-cation interactions are ig-

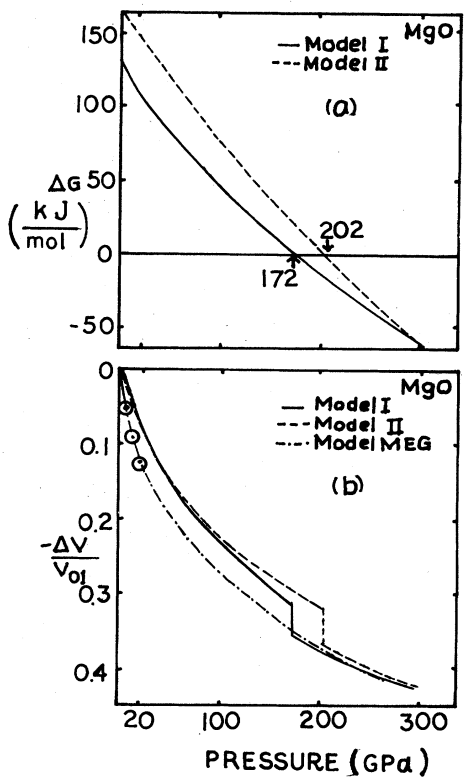

FIG. 1. (a) Variation of ΔG with pressure for MgO. (b) Phase diagram of MgO. ○ are experimental points, taken from Ref. 19.

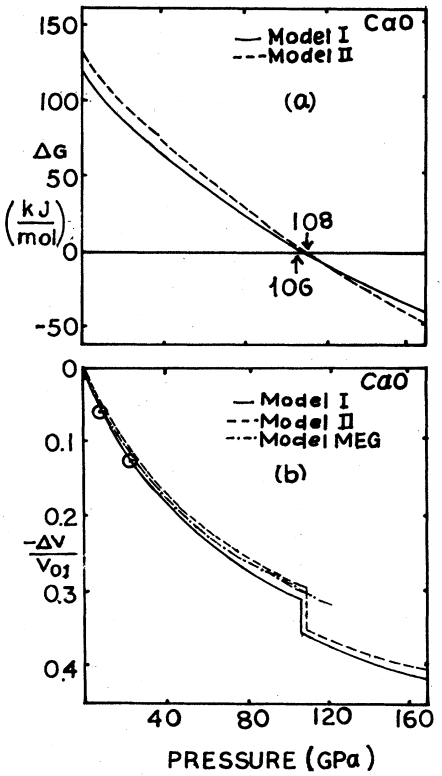

FIG. 2. (a) Variation of ΔG with pressure for CaO. (b) Phase diagram of CaO. ○ are experimental points, taken from Ref. 19.

nored while for anion-cation potentials no van der Waals terms are included. In contrast, the potential in model II is more appropriate as it allows the parameters B_{ij} and ρ_{ij} and C_{ij} to attain different values for the different oxides. Moreover, their evaluation has been done in the spirit of microscopic models. In our study with the models I and II, we have directly used the values of these parameters, reported by Sangster and Stoneham[14] and Mackrodt and Stewart,[15] respectively.

III. STRUCTURAL PHASE TRANSITION

For the assessment of relative stability of $B1$ and $B2$ structures, we have minimized the cohesive energies given by Eqs. (4) and (5) and consequently obtained the equilibrium values of R and R'. Their values and the corresponding Gibbs free energies U_{B1} and U_{B2} together with their difference ΔU $(=U_{B2}-U_{B1})$ are listed in Table I. The cohesive energies obtained from model I and model II are in closer agreement with their measured data[16–18] as is obvious from Table I. Moreover, the positive values of ΔU for all the oxides indicate that both the models have correctly predicted their relative stability of crystal structures. In order to predict the transition pressure, we have minimized the Gibbs free energy with respect to interionic separations and calculated ΔG $(G_{B2}-G_{B1})$ for various pressures. As the pressure is increased, these values of ΔG decrease and approach zero at the transition pressure. Beyond this pressure ΔG becomes negative as the phase $B2$ becomes more stable. The variation of ΔG with pressure for all the oxides has been plotted in Figs. 1(a)—8(a) for models I and II. The phase-transition pressures obtained from these calculations are presented in Table II and compared with other theoretical[1] and experimental[2,3] results.

The first-order phase transition involving a discontinuity in volume takes place at the transition pressure. Experimentally one usually studies the relative volume changes $(-\Delta V/V_{01})$ associated with the compressions. These are defined as the negative of the difference between the volume of the more stable phase at a given pressure and the volume V_{01} of $B1$ phase at zero pressure divided by V_{01}. The magnitude of the discontinuity in $-\Delta V/V_{01}$ at the transition pressure is obtained from the phase diagrams and their values for different oxides for both the models are listed in Table II. The phase diagrams are depicted in Figs. 1(b)—8(b). In these phase dia-

TABLE I. Cohesive properties and stability of divalent metal oxides ($B1$ and $B2$ phases at 0 K).

Crystal	Model	Equilibrium separation (10^{-1} nm) $R(B1)$	$R(B2)$	Cohesive energy (kJ/mole) $U(B1)$	$U(B2)$	ΔU (kJ/mole) $[U(B2)-U(B1)]$
MgO	I	2.12	2.23	−3936	−3806	130
	II	2.19	2.32	−3885	−3722	163
	Expt.	2.106[a]		−3898[b]		
	MEG	2.29[b]	2.43[c]	−3647[c]		
CaO	I	2.41	2.54	−3458	−3341	117
	II	2.47	2.61	−3454	−3320	134
	Expt.	2.405[a]		−3475[b]		
	MEG	2.47[c]	2.61[c]	−3412[c]		
SrO	I	2.59	2.73	−3213	−3099	114
	II	2.63	2.77	−3258	−3141	117
	Expt.	2.580[a]		−3262[b]		
BaO	I	2.77	2.93	−2993	−2882	111
	II	2.78	2.95	−3083	−2968	115
	Expt.	2.761[a]		−3079[b]		
MnO	I	2.23	2.36	−3719	−3589	130
	II	2.43	2.56	−3530	−3394	136
	Expt.	2.222[a]		−3813[d]		
FeO	I	2.17	2.28	−3848	−3719	129
	II	2.40	2.53	−3576	−3440	136
	Expt.	2.155[a]		−3928[d]		
CoO	I	2.14	2.25	−3931	−3813	118
	Expt.	2.133[a]		−3996[d]		
NiO	I	2.09	2.20	−4018	−3897	121
	Expt.	2.084[a]		−4083[d]		

[a]Reference 16.
[b]Reference 17.
[c]Reference 1.
[d]Reference 18.

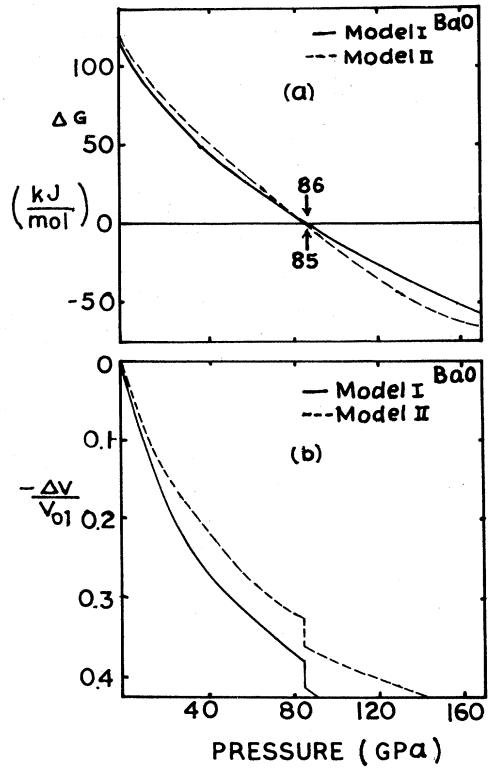

FIG. 3. (a) Variation of ΔG with pressure for BaO. (b) Phase diagram of BaO.

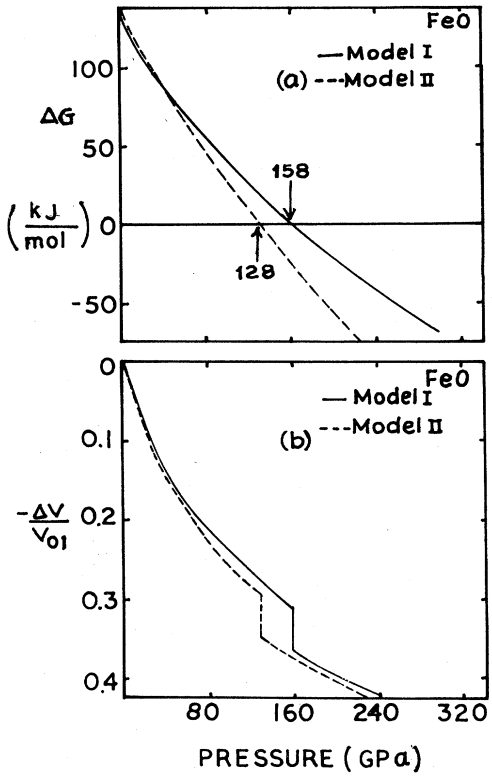

FIG. 5. (a) Variation of ΔG with pressure for FeO. (b) Phase diagram of FeO.

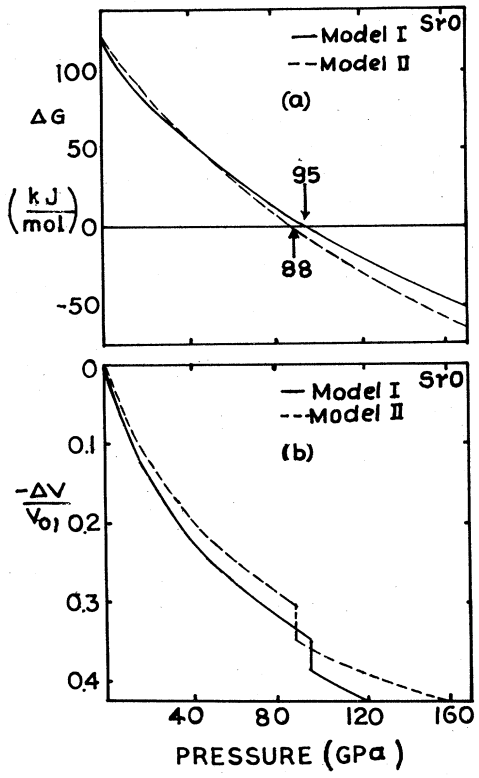

FIG. 4. (a) Variation of ΔG with pressure for SrO. (b) Phase diagram of SrO.

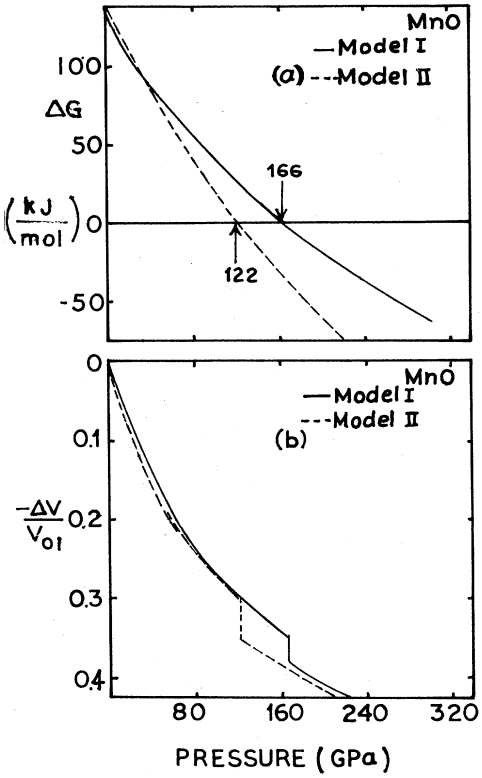

FIG. 6. (a) Variation of ΔG with pressure for MnO. (b) Phase diagram of MnO.

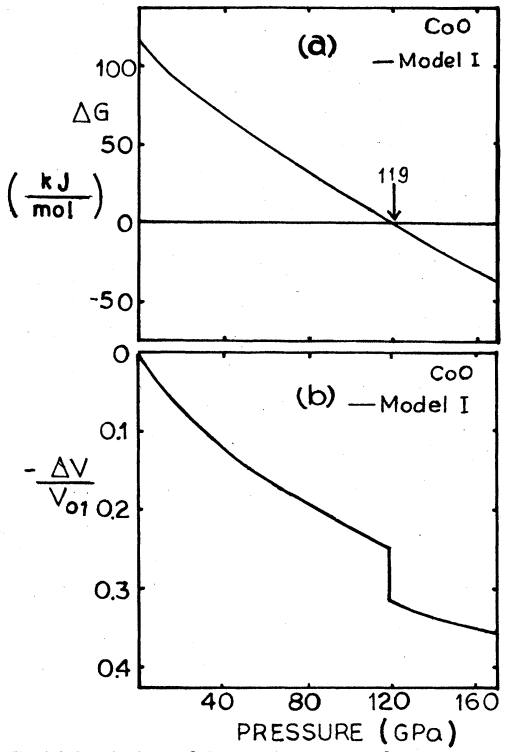

FIG. 7. (a) Variation of ΔG with pressure for CoO. (b) Phase diagram of CoO.

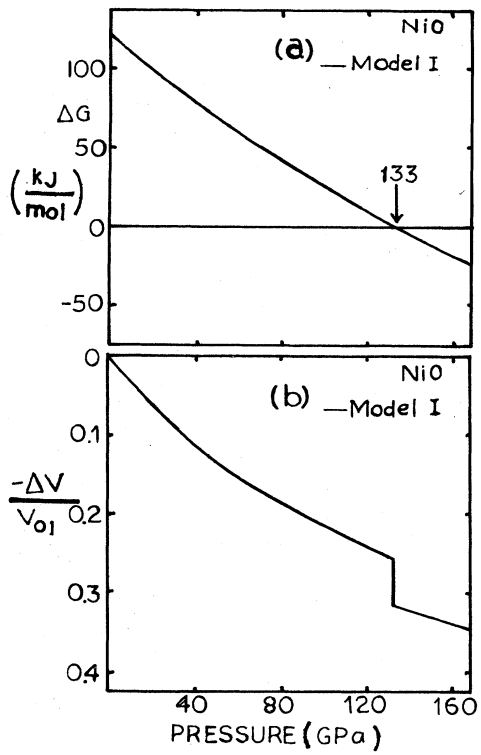

FIG. 8. (a) Variation of ΔG with pressure for NiO. (b) Phase diagram of NiO.

TABLE II. High-pressure behavior of divalent metal oxides at 0 K.

Crystal	Model	Transition pressure (GPa) $B1 \rightarrow B2$	Shear instability (GPa)	Volume changes for $B1 \rightarrow B2$ transition $-\frac{\Delta V_{B1}}{V_{01}}$	$-\frac{\Delta V_{B2}}{V_{01}}$	$-\frac{\Delta V_t}{V_{01}}$	Relative change in volume (%)
MgO	I	172	295	0.313	0.355	0.042	4.2
	II	202	765	0.323	0.373	0.050	5.0
	MEG	256[a]	555[a]				
CaO	I	106	173	0.313	0.360	0.047	4.7
	II	108	328	0.300	0.355	0.055	5.5
	Expt.	70±10[b]					11.0[b]
	MEG	121[a]	342[a]				
SrO	I	95	143	0.348	0.388	0.040	4.0
	II	88	253	0.303	0.348	0.045	4.5
	Expt.	36±4[c]					13.0[c]
BaO	I	86	113	0.380	0.413	0.033	3.3
	II	85	373	0.325	0.360	0.035	3.5
MnO	I	166	258	0.345	0.383	0.038	3.8
	II	122	363	0.300	0.353	0.053	5.3
FeO	I	158	283	0.310	0.363	0.053	5.3
	II	128	340	0.293	0.348	0.055	5.5
	Expt.	~90[b]					~4.0[b]
CoO	I	119	270	0.250	0.315	0.065	6.5
NiO	I	133	298	0.253	0.315	0.062	6.2

[a]Reference 1.
[b]Reference 2.
[c]Reference 3.

TABLE III. Static elastic properties of divalent metal oxides ($B1$ phase at 0 K).

Crystal	Model	C_{11} (GPa)	$C_{12}=C_{44}$ (GPa)	B (GPa)	$\left[\frac{dC_{11}}{dP}\right]_0$	$\left[\frac{dC_{12}}{dP}\right]_0$	$\left[\frac{dC_{44}}{dP}\right]_0$	$\left[\frac{dB}{dP}\right]_0$	$\frac{C_{44}}{B}$ at predicted P_t
MgO	I	364	157	222	7.56	1.76	−0.09	3.70	0.11
	II	290	193	216	7.12	2.28	0.49	3.89	0.22
	Expt.	289[a]	155[a]	168.8[b]	8.7[b]	1.5[b]	1.0[b]	3.8[b]	
		310[b]	160[b]						
	MEG	225.7[b]	142.4[b]	170.2[b]	7.24[b]	2.41[b]	0.41[b]	4.02[b]	
CaO	I	219	94	135	6.70	1.60	−0.08	3.30	0.11
	II	212	105	138	7.62	2.09	0.22	3.93	0.18
	Expt.	226[c]	81[c]	112[d]	10.5[b]		0.60[b]	6.0[b]	
		223[b]	83[b]	114[b]		3.70[b]		4.8[d]	
	MEG	207[b]	97[b]	133[b]	7.89[b]	2.19[b]	0.19[b]	4.09[b]	
SrO	I	154	71	98	7.10	1.79	−0.05	3.56	0.08
	II	186	78	113	8.79	2.23	0.12	4.41	0.15
	Expt.	173[e]	56[e]					4.4[f]	0.174[g]
								5.2[h]	
BaO	I	110	55	73	2.95	0.79	−0.01	1.51	0.06
	II	150	61	91	8.32	2.12	0.16	4.17	0.14
	Expt.	126[h]	34[h]						
MnO	I	276	128	175	7.26	1.81	−0.06	3.62	0.08
	II	259	111	158	6.87	1.71	0.13	3.43	0.16
	Expt.	223[i]	79[i]						
FeO	I	332	144	203	9.02	2.12	−0.11	4.42	0.11
	II	282	116	169	9.49	2.29	0.15	4.69	0.15
	Expt.	359[j]	56[j]	185[k]				3.2[d]	
CoO	I	412	149	234	8.54	1.76	−0.18	4.02	0.15
	Expt.	256[l]	80[l]						
NiO	I	446	163	254	9.44	1.96	−0.19	4.45	0.15
	Expt.	270[l]	105[l]						

[a]Reference 29.
[b]Reference 1.
[c]Reference 30.
[d]Reference 2.
[e]Reference 31.
[f]Reference 8.
[g]Reference 3.
[h]Reference 32.
[i]Reference 33.
[j]Reference 34.
[k]Reference 36.
[l]Reference 35.

grams, the curve below the transition pressure is the compression curve for the $B1$ phase; the curve above the transition pressure is the same compression curve corresponding to the $B2$ phase. In Figs. 1(b)—8(b) we have compared the results obtained from models I and II. In the cases of MgO and CaO, we have also compared our results with those of Cohen and Gordon[1] who have obtained them from a modified electron-gas model (MEG) and experimental data, corresponding to low pressures.[19]

IV. HIGH-PRESSURE ELASTIC BEHAVIOR

The study of the elastic constants (C_{11}, C_{12}, and C_{44}) of ionic solids and their pressure derivatives $(dC_{ij}/dP)_0$ at zero pressure and 0 K is quite important for understanding the nature of the interionic forces[20] in them. Since these elastic constants[21] are functions of the first- and second-order derivatives of the short-range (SR) potentials $[V_{ij}(r)]$, their calculations will provide a further check on the accuracy of SR forces in these solids. This motivated us to calculate the elastic constants for a static lattice at 0 K at various applied pressures and investigate their pressure variations.

In order to compute these elastic constants, it is useful to partition them into the contributions from Coulombic and SR forces. Thus, we have expressed $C_{ij}=C_{ij}^{\text{Coul}}+C_{ij}^{\text{SR}}$, $i,j=1,2$. The Coulombic contributions obtained by Cowley[22] are given by

$$C_{11}^{\text{Coul}}=-(2.55604)e^2Z^2/2R^4\,, \tag{7}$$

$$C_{12}^{\text{Coul}}=(0.11298)e^2Z^2/2R^4\,, \tag{8}$$

$$C_{44}^{\text{Coul}}=(1.27802)e^2Z^2/2R^4\,. \tag{9}$$

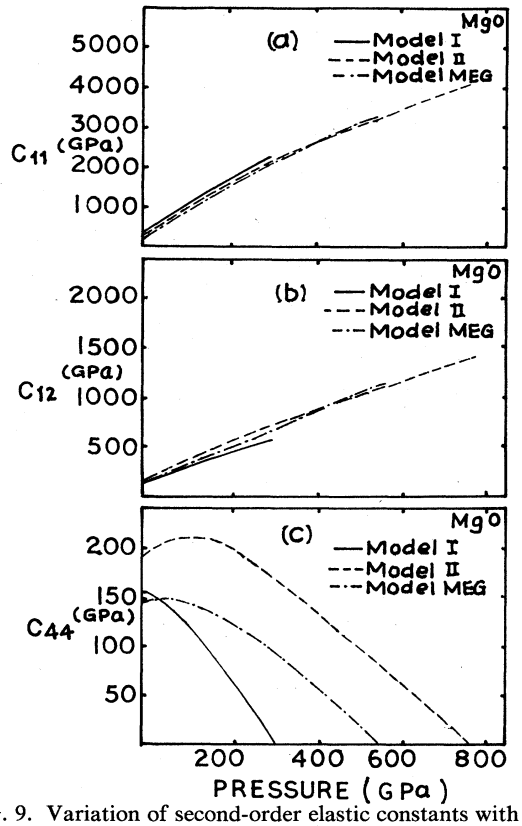

FIG. 9. Variation of second-order elastic constants with pressure for MgO. (a) C_{11}; (b) C_{12}; (c) C_{44}.

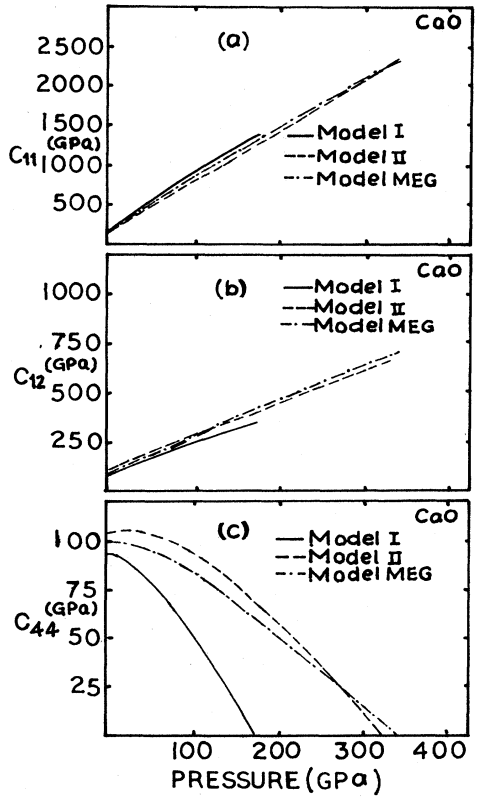

FIG. 10. Variation of second-order elastic constants with pressure for CaO. (a) C_{11}; (b) C_{12}; (c) C_{44}.

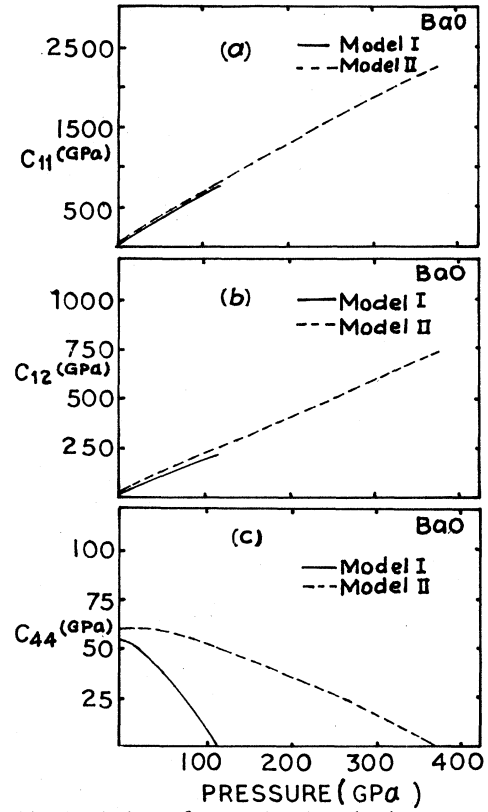

FIG. 11. Variation of second-order elastic constants with pressure for BaO. (a) C_{11}; (b) C_{12}; (c) C_{44}.

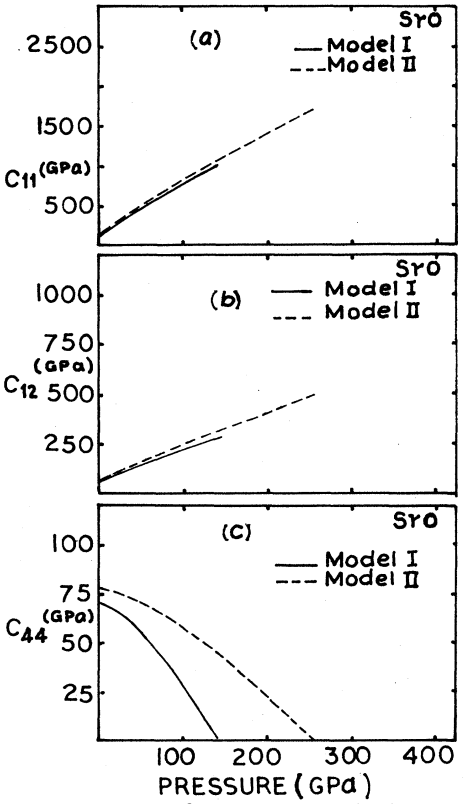

FIG. 12. Variation of second-order elastic constants with pressure for SrO. (a) C_{11}; (b) C_{12}; (c) C_{44}.

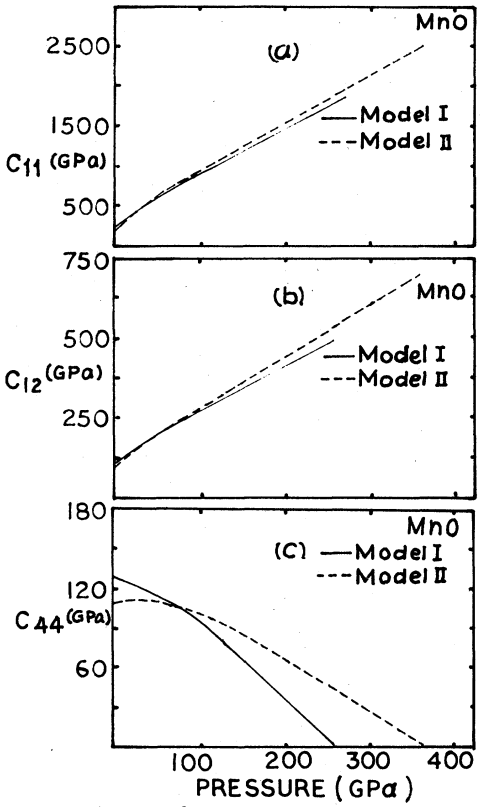

FIG. 13. Variation of second-order elastic constants with pressure for MnO. (a) C_{11}; (b) C_{12}; (c) C_{44}.

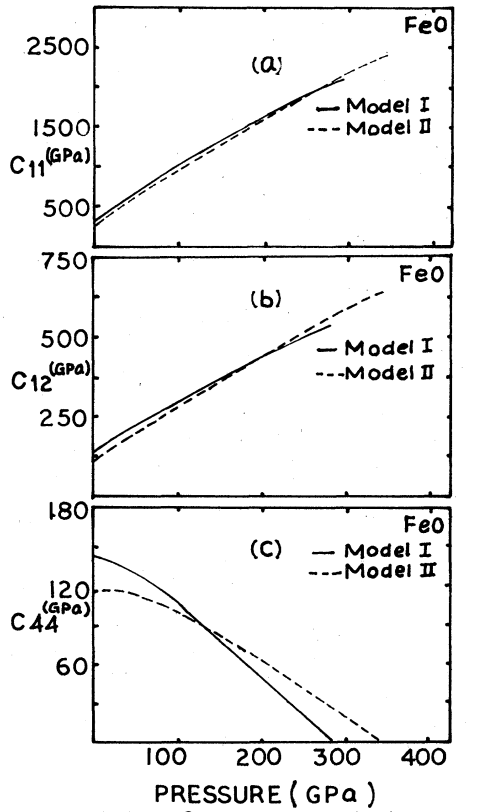

FIG. 14. Variation of second-order elastic constants with pressure for FeO. (a) C_{11}; (b) C_{12}; (c) C_{44}.

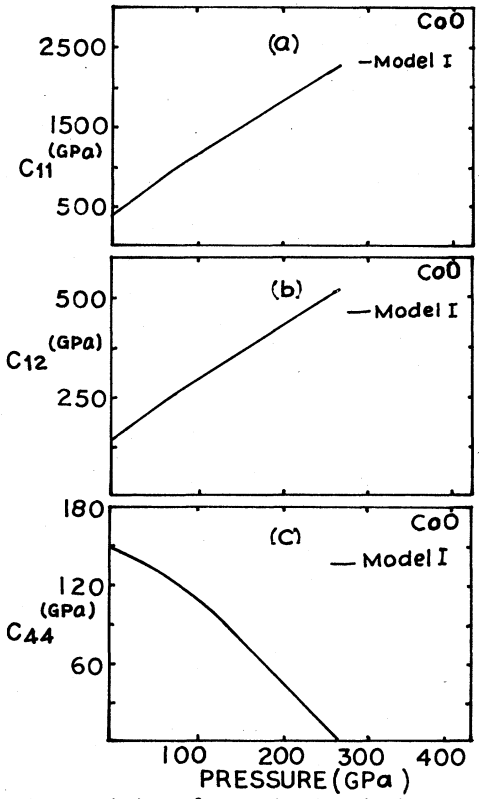

FIG. 15. Variation of second-order elastic constants with pressure for CoO. (a) C_{11}; (b) C_{12}; (c) C_{44}.

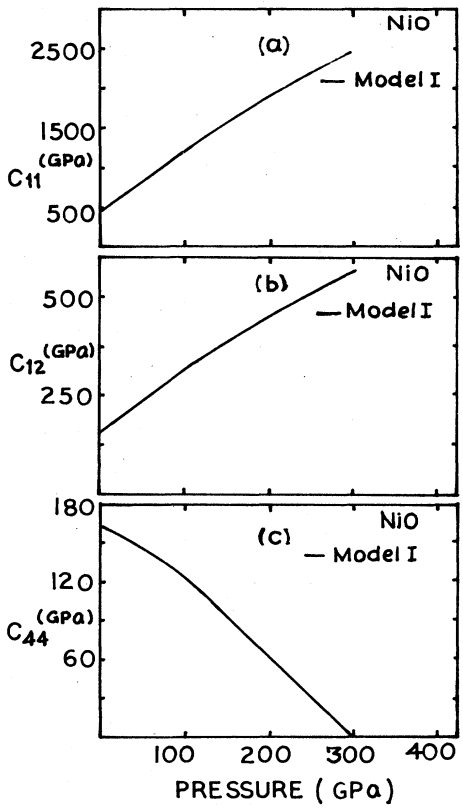

FIG. 16. Variation of second-order elastic constants with pressure for NiO. (a) C_{11}; (b) C_{12}; (c) C_{44}.

The SR contributions restricted to first- and second-nearest-neighbor interactions are

$$C_{11}^{SR}=\frac{1}{R}\left[\frac{d^2V_{+-}}{dr^2}\right]_{r=R}+\frac{1}{R}\left[\frac{d^2(V_{++}+V_{--})}{dr^2}\right]_{r=\sqrt{2}R}+\frac{1}{\sqrt{2}R^2}\left[\frac{d(V_{++}+V_{--})}{dr}\right]_{r=\sqrt{2}R}, \tag{10}$$

$$C_{12}^{SR}=-\frac{1}{R^2}\left[\frac{dV_{+-}}{dr}\right]_{r=R}+\frac{1}{2R}\left[\frac{d^2(V_{++}+V_{--})}{dr^2}\right]_{r=\sqrt{2}R}-\frac{5}{2\sqrt{2}R^2}\left[\frac{d(V_{++}+V_{--})}{dr}\right]_{r=\sqrt{2}R}, \tag{11}$$

$$C_{44}^{SR}=\frac{1}{R^2}\left[\frac{dV_{+-}}{dr}\right]_{r=R}+\frac{1}{2R}\left[\frac{d^2(V_{++}+V_{--})}{dr^2}\right]_{r=\sqrt{2}R}+\frac{3}{2\sqrt{2}R^2}\left[\frac{d(V_{++}+V_{--})}{dr}\right]_{r=\sqrt{2}R}, \tag{12}$$

where r is the appropriate distance variable for each pair.

The results for the total elastic constants and bulk modulus B $[=\frac{1}{3}(C_{11}+2C_{12})]$ at 0 K and zero applied pressure computed from models I and II are listed in Table III and compared with the available experimental data. Their pressure derivatives at zero applied pressure have also been evaluated by a finite-difference approximation in the range 0—1 GPa and are listed in Table III. The study of the elastic constants, bulk modulus, and shear-to-bulk modulus ratio (C_{44}/B) as a function of pressure is of great importance, since they govern the high-pressure behavior of oxides. For example, the pressure at which a shear instability ($C_{44}=0$) occurs can be taken to represent an upper bound on the transition pressure of these crystals from the $B1$ phase to a more densely packed phase, presumably $B2$. In order to determine the shear instability and monitor the high-pressure behavior of all the effective elastic constants, the equations (7) to (12) for C_{11}, C_{12}, and C_{44} are evaluated at the appropriate equilibrium separations for various pressures and the results are graphically presented in Figs. 9—16. The values of shear instability obtained from models I and II are collected in Table II. The values of C_{44}/B at the predicted transition pressures are tabulated in the last column of Table III to check the validity of the modified Born stability criterion.[23]

V. DISCUSSION AND CONCLUSION

A look at Table I shows that the present models I and II have given results for equilibrium separations and cohesive energies in good agreement with their experimental values[16–18] although the comparison of the present results with experimental data is made difficult by the fact that the available data correspond to room temperature whereas the calculations pertain rigorously to 0 K. However, the agreements achieved by us are better than those obtained from MEG model in the cases of MgO and CaO. Also, the predictions from model II for MnO and FeO are not as satisfactory as those from model I. It is interesting to note that both the models I and II have correctly predicted the relative stability of competitive structures as ΔU obtained from them (see last column of Table I) are positive (which is the required criterion[24]) for all metal oxides. The larger values of ΔU for these oxides (ranging from 111 to 163 kJ/mol) as compared to those obtained for alkali halides[25] indicate that these oxides will have higher phase transition pressure then those for the alkali halides. Thus, the high values (ranging from 85 to 202 GPa) of transition pressures predicted by us for oxides and those obtained by Cohen and Gordon[25] for alkali halides are consistent with their expectation. An inspection of Table II (first column) and Figs. 1(a)—8(a) shows that the transition pressures predicted by model II increases in the order BaO (85 BPa), SrO (88 GPa), CaO (108 GPa), MnO (122 GPa), FeO (128 GPa), and MgO (202 GPa) with decreasing cation—to—anion-radii ratio. This is in keeping with the correlation of transition pressures in $B1$ monoxides with radius ratio quoted by Jeanloz and Ahrens.[2] The predictions from model I have also followed the same trend in all other oxides except for MnO and FeO. Numerical values of the transition pressures predicted by both the models and those from MEG model[1,13] are, however, higher than the corresponding available experimental values.

Earlier, Vukcevich[26] proposed a high-pressure stability criterion for ionic crystals, combining mechanical stability with minimum energy conditions. According to him, the stable phase of the crystal is one in which the shear elastic constant C_{44} is nonzero (for mechanical stability) and which has the lowest potential energy among the mechanically stable lattices. Also, the pressure at which $C_{44}=0$ (i.e., shear instability) indicates the upper bound for the transition pressure. Thus, a look at the second column of Table II indicates that for both the models and for all the oxides the shear instability is higher than the corresponding transition pressures. This supports the high-pressure stability criterion proposed by Vukcevich.[26]

The phase diagrams for divalent metal oxides shown in Fig. 1(b)—8(b) are found to exhibit the discontinuities in the volume indicating a drastic structural change at the phase-transition pressure obtained at a point, where $\Delta G=0$, in the ΔG-versus-P graphs shown in the Figs. 1(a)—8(a). This is the characteristic of the first-order phase transition in these oxides. For MgO and CaO, the compression curves for the $B1$ phase obtained by Cohen and Gordon from the MEG model[1] are also drawn in Figs. 1(b) and 2(b) for comparison, along with the low-pressure experimental data.[19] Our results for model II for CaO are almost the same as for the MEG model and experimental values. However, both models I and II have predicted higher values than the experimental and MEG values for MgO. The relative changes in volume at the predicted transition computed from the curves [Figs. 1(b)—8(b)] range from 3.3% to 6.5% while the experimental values are 11% for CaO, 13% for SrO, and 4% for FeO. The reason for this discrepancy is not well known, but it might be due to the neglect of many-body forces[27,28]

which are volume forces.[28] In Table III we have presented the calculated values of C_{11}, C_{12}, and C_{44} along with their experimental values[29–36] for comparison. Our results show reasonable agreement for C_{11}, while for C_{12} and C_{44} they are higher than the experimental values. This might also be due to the exclusion of many-body effects which are directly responsible for the Cauchy discrepancy[20] between the elastic constants ($C_{12} \neq C_{44}$). We have also studied the pressure variation of these elastic constants up to the pressure corresponding to the shear instability, and results are displayed in Figs. 9–16. For all the oxides, it may be noted that the elastic constants C_{11} and C_{12} monotonically increase with pressure, while C_{44} initially increases, reaches a maximum, and then decreases steadily almost at a constant rate and eventually becomes zero at sufficiently high pressure. The shear instability obtained from graphing [Figs. 9(c) to 16(c)] is noted in the second column of Table II. The variation of C_{11}, C_{12}, and C_{44} with pressure predicted by models I and II is found to follow the same trend as that predicted by Cohen and Gordon[1] for MgO and CaO. Their results are also plotted for comparison. Model-I predictions for C_{44}, however, do not indicate the initial increase of C_{44} with pressure. In fact, for all oxides the calculated values of the pressure derivatives of C_{44} at zero pressure; $(dC_{44}/dP)_0$ from model I are negative while their values from model II, the MEG model, and measurements are positive. The values of calculated zero pressure derivatives of the elastic constants listed in Table III compare reasonably well with their MEG predictions and available experimental data.[2,3,8] However, both the models for BaO do not follow the general trend. The values of C_{44}/B at the predicted transition pressure for all the oxides range from 0.06 to 0.22 as is noted in the last column of Table III.

Although our results for both the transition pressure and volume decrease at the $B1$-to-$B2$ transition are not in closer agreement with their measured data, they have followed systematic and similar trends exhibited by the oxides[2] and are comparable to those obtained from the modified electron-gas model.[1] The discrepancies between our theoretical and available experimental results may be associated with the many-body interactions whose effects are important in crystals with widely different ion sizes,[27,28] as indicated earlier.

The two model potentials which we have employed were originally formulated to study the lattice dynamics and defect properties of divalent metal oxides. In the present work, we have successfully extended them for the study of pressure-induced phase transition and high-pressure behavior of these oxides. A major finding of this study is that the results of model I, which is phenomenological and simple, are surprisingly more or less identical to those achieved from relatively more sophisticated model II and MEG model, whose parameters are derived from the *ab initio* approach. This is quite encouraging since the reasonably successful study can be made from the simple model I without the loss of generality and without withholding the work on the solids because of a lack of model parameters determined from an *ab initio* approach.

ACKNOWLEDGMENT

The authors are thankful to University Grants Commission, New Delhi, for providing financial support to this project.

*Permanent address: Department of Physics, Mohanlal Hargovinddas College of Home Science, Rani Durgawati University, Jabalpur 482001, Madhya Pradesh, India.

†Department of Physics, Faculty of Physical Sciences, Bhopal University, Bhopal, 462026, India.

[1] A. J. Cohen and R. G. Gordon, Phys. Rev. B **14**, 4593 (1976).

[2] R. Jeanloz and T. J. Ahrens, Geophys. J. R. Astr. Soc. **62**, 505 (1980).

[3] Y. Sato and R. Jeanloz, J. Geophys. Res. **86**, 11773 (1981).

[4] M. S. T. Bukowinski and J. Hauser, Geophys. Res. Lett. **7**, 689 (1980).

[5] Z. P. Chang and E. K. Graham, J. Phys. Chem. Solids **38**, 1355 (1977).

[6] R. Jeanloz, T. J. Ahrens, H. K. Mao, and P. M. Bell, Science **206**, 829 (1979).

[7] J. A. Tossell, J. Geophys. Res. **85**, 6456 (1980).

[8] L. G. Liu and W. A. Bassett, J. Geophys. Res. **78**, 8470 (1973).

[9] L. G. Liu and W. A. Bassett, J. Geophys. Res. **77**, 4934 (1972).

[10] H. K. Mao and P. M. Bell, J. Geophys. Res. **84**, 4533 (1979).

[11] P. R. Son and R. A. Bartels, J. Phys. Chem. Solids **33**, 819 (1972).

[12] K. H. Rieder, B. A. Weinstein, M. Cardona, and H. Bilz, Phys. Rev. B **8**, 4780 (1973).

[13] C. W. Muhlhausen and R. G. Gordon, Phys. Rev. B **23**, 900 (1981).

[14] M. J. L. Sangster and A. M. Stoneham, Atomic Energy Research Establishment (Harwell) Report No. TP-833 (1980) (unpublished).

[15] W. C. Mackrodt and R. F. Stewart, J. Phys. C **12**, 431 (1979).

[16] R. W. G. Wyckoff, *Crystal Structures* (Wiley, New York, 1963), Vol. 1.

[17] G. V. Samsonov, *The Oxide Handbook* (Plenum, New York, 1973).

[18] T. C. Waddington, Adv. Inorg. Radio Chem. **1**, 157 (1959).

[19] E. A. Perez Albuerene and H. G. Drickmar, J. Chem. Phys. **43**, 1381 (1965).

[20] M. P. Tosi, Solid State Phys. **16**, 1 (1964).

[21] H. B. Huntington, Solid State Phys. **7**, 213 (1958).

[22] R. A. Cowley, Proc. R. Soc. London, Ser. A **268**, 121 (1962).

[23] A. J. Miller, G. A. Saunders, and Y. K. Yoğurtcu, J. Phys. C **14**, 1569 (1981).

[24] M. J. L. Sangster, U. Schroder, and R. M. Atwood, J. Phys. C **11**, 1523 (1978).

[25] A. J. Cohen and R. G. Gordon, Phys. Rev. B **12**, 3228 (1975).

[26]M. R. Vukcevich, Phys. Status Solidi B **54**, 435 (1972).
[27]P. O. Löwdin, Philos. Mag. Suppl. **5**, 1 (1956).
[28]R. K. Singh, Phys. Rep. (Netherlands) **85**, 259 (1982).
[29]D. H. Chung, Philos. Mag. **8**, 833 (1963).
[30]A. L. Dragoo and I. L. Spain, J. Phys. Chem. Solids **38**, 705 (1977).
[31]R. A. Bartels and P. R. Son, Bull. Am. Phys. Soc. **16**, 357 (1971).
[32]Z. P. Chang and E. K. Graham, J. Phys. Chem. Solids **38**, 1355 (1977).
[33]D. W. Oliver, J. Appl. Phys. **40**, 893 (1969).
[34]G. Kugel, C. Carabatos, B. Hennion, B. Prevot, A. Revcolevschi, and D. Tocchetti, Phys. Rev. B **16**, 378 (1977).
[35]N. Uchida and S. Saito, J. Acad. Soc. Am. **51**, 1602 (1971).
[36]I. Jackson, R. C. Libermann, and A. E. Ringwood, Phys. Chem. Miner. **3**, 11 (1978).